Authors

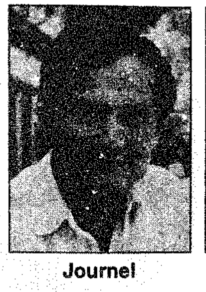

Journel

Gómez-Hernández

André G. Journel, professor of geostatistics and petroleum engineering, is director of the Stanford Center for Reservoir Forecasting in Stanford, CA. His research includes stochastic characterization of reservoir heterogeneities and integration of hard and soft data from various sources and scales, accounting for various degrees of reliability. **J. Jaime Gómez-Hernández** is a research professor at the Polytechnic U. of Valencia, working on analysis of uncertainty of groundwater model predictions in relation to nuclear waste disposal.

Subscripts

i,j,k,l = stratigraphic coordinates
x,y,z = Cartesian Coordinates

Acknowledgments

We gratefully acknowledge Exxon Co. U.S.A. for providing data from part of the Wilmington oil field. Financial support for this project was provided by the Stanford Center for Reservoir Forecasting.

References

1. Journel, A.G. and Alabert, F.G.: "Non-Gaussian Data Expansion in the Earch Sciences," *Terra Nova* (1989) **1(2)**, 123–34.
2. Journel, A.G. and Alabert, F.G.: "New Method for Reservoir Mapping," *JPT* (Feb. 1990) 212–18.
3. Gómez-Hernández, J.J. and Srivastava, R.M.: "ISIM3D: A Three-Dimensional Multiple Indicator Conditional Simulation Program," *Computers & Geosciences* (1990) **16(4)**, 395–440.
4. Mayuga, M.N.: "Geology and Development of California's Giant—Wilmington Oil Field," *Geology of Giant Petroleum Fields*, AAPG Memoirs 14 (1970) 158–84.
5. Jones, T.A., Hamilton, D.E., and Johnson, C.R.: *Contouring Geological Surfaces With the Computer*, Van Nostrand, New York City (1986) 102–13.
6. Hewett, T. and Behrens, R.: "Conditional Simulations of Reservoir Heterogeneities With Fractals," *SPEFE* (Sept. 1990) 217–25; *Trans.*, AIME, **289**.

SPEFE

Original SPE manuscript received for review Oct. 8, 1989. Revised manuscript received March 17, 1992. Paper accepted for publication May 7, 1992. Paper (SPE 19857) first presented at the 1989 SPE Annual Technical Conference and Exhibition held in San Antonio, TX, Oct. 8–11.

Microseismic Logging: A New Hydraulic Fracture Diagnostic Method

Kenneth D. Mahrer,* SPE, Teledyne Geotech

Summary. Hydraulic fracture treatments and fluid injections into fractured wells induce a useful cloud of microseismic sources in the fractured zone. This induced seismicity can last for hours after pumping and pervades the fracture. The source-size population distribution ranges from a countable (50 to 500) number of large, individually distinguishable events to a din of background events. Each source radiates wave motion, which can be recorded only in and near the fracture. A new method uses these motion data, recorded in the cased treatment well, to determine the fracture height and azimuth. The height is found by delineating the location and vertical extent of a spatial anomaly in the background-motion data. The azimuth is derived from the particle-motion polarization of the largest events of the microseismic event population. This paper describes the method, exemplary data sets, theory, and simulations that substantiate this method.

Introduction

Two questions frequently occur during hydraulic fracturing of cased wells: In what direction did the fracture grow (i.e., the fracture azimuth), and What is the size of the fractured region? A new diagnostic method, *microseismic logging*, can answer the first question and partially answer the second. It can determine the fracture azimuth and height with information derived directly from the fracture.

Hydraulic fracture treatments induce sudden small shifts or adjustments (i.e., microseismic events or microearthquakes) in the fractured zone. Events also can be triggered by repressurizing or depressurizing (e.g., venting and backflowing) a previously fractured formation. The loci of sources or hypocenters form a pervasive cloud covering the fracture. These sources radiate waves, which can be recorded and used as diagnostic tools for fracture imaging.

The microseismicity begins during treatments, pressurization, or depressurization and continues for a few hours afterward. In all cases, the microseismicity or radiated seismic energy is low and the resulting waveforms can be recorded only in the treated well or nearby (i.e., closer than a few hundred meters) wells. Because nearby or observation wells at this range are atypical, fracture diagnostic methods had to be developed to use the induced microseismicity or signals recorded in the treated well.

Method

Microseismic data recorded in the treated well differ substantially from data recorded outside the well. Outside the well, the data are similar to those recorded from earthquakes. These data show well-defined body wave phases (P and S waves) that can be used to find and analyze microseismic sources. In the treated well, these phases do not appear and other methods have had to be used or developed.

Treatment well motion data divides into three categories. Category 1 includes the easily identified, high-amplitude, discrete signals that can be attributed to the fracture environment. Category 2 is the background motion. Its distinction from the signals is somewhat arbitrary and is manifested as a heightened amplitude level above the pretreatment or prepumping noise. The background is composed of signals whose sources are too small to distinguish individually but belong to the continuous population or cloud of seismic activity in the fractured zone.

Category 3 is the noise or that part of the recorded data that cannot be attributed to the treatment or fractured environment. Like noise in any data set, this is the component that obscures the information content. During processing, noise removal or reduction is a constant battle.

We use the signals to determine azimuth and the background motion to determine fracture height. We use the background motion without signals because its height-determining character remains stationary and it is distributed more smoothly and continuously over the fractured volume than the loci of large events. If processing included signals and background, the background energy would be overwhelmed by the signal energy, which is not volumetrically pervasive and, hence, does not contain height information.

The background without discrete signals, or simply the background motion, profoundly changes character as a function of recording depth in the treated well. This anomaly is a direct result of the fracture and overlays the change in in-situ properties produced by the fracturing. The anomaly maps the vertical expression or, equivalently, fracture height. To identify the anomaly in the data, we must record the seismicity over a range of depths that extends beyond the fracture. From data recorded at each depth, we isolate the background motion between large events and separate it into two components: the average horizontal amplitude, A_H, and the average vertical amplitude, A_V. We separate the background motion because the background anomaly is identified best in the component behavior. A_H is greater at recording depths in the fracture, and A_V is greater outside (above and below) the fracture. From the components, we calculate and plot the component ratio, A_H/A_V, as a function of recording depth and identify where the ratio inverts. The inversion points give the fracture height limits. The A_H/A_V ratio is a robust method. Use of a ratio of components adds some benefits.

The A_H/A_V method overcomes some common problems in borehole seismic recording. The ratio reduces the noise. The A_H/A_V anomaly or excursion is unaffected by reasonable mismatches in geophone components. The geophone properties are consistent throughout the entire recording traverse and will not affect a ratio. Similarly, locking force is an insignificant issue. At each recording depth, we lock the tool and slack the wireline. Because the locking mechanism supports the tool, the locking force exceeding tool weight stiffens the tool and the casing, which represents an insignificant change in ratio response.

In contrast to the height determination, the fracture azimuth is determined from the discrete signals. We use the discrete signals because the azimuth calculation is sensitive to noise and the signals have strong signal/noise ratios.

Because the azimuth method is not well-known in petroleum engineering, I will give a short summary. First, we isolate the signals from the data set. Then, we determine the particle-motion direction or polarization of the initial phase of each signal. We use only the initial phase for two reasons. First, this part of the signal is polarized in the motion direction of the propagating waves. Second, after this point, the signals also may be contaminated by the wobbling or resonances of the recording tool.[1]

From the polarizations, we delineate the directions or vectors to the sources of the signals. In general, these vectors cluster along the principal direction of the source cloud. Because seismic sources lie in a tabular-shaped fractured zone and because the wellbore runs directly through the source cloud, the direction to the microseismic sources from the well defines the fracture azimuth.

Seismic polarization analysis is an established and proven seismic diagnostic tool[2] so I will not discuss it. Except for the data-acquisition description below, the remainder of this paper is devoted to height determination.

*Now at Southwest Research Inst.

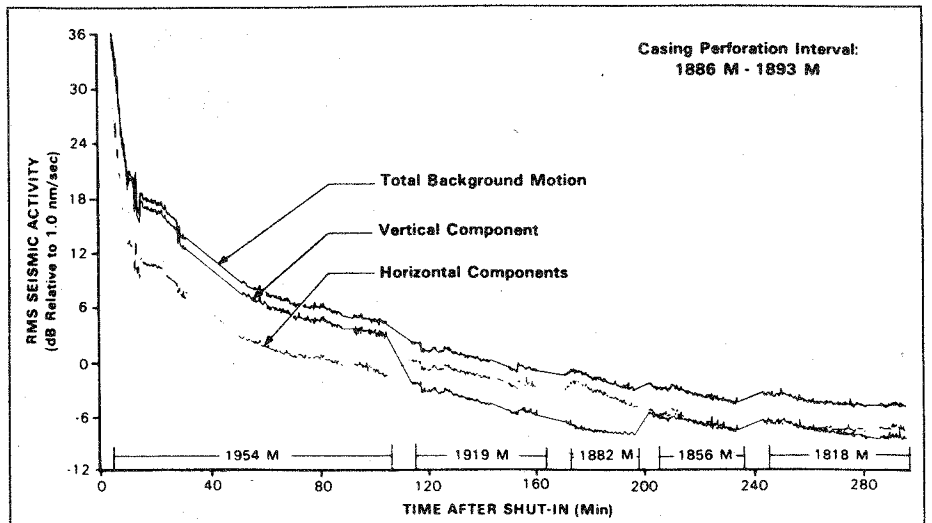

Fig. 1—RMS amplitudes of background motion at SFE 1 vs. time relative to shut-in and associated recording depths.

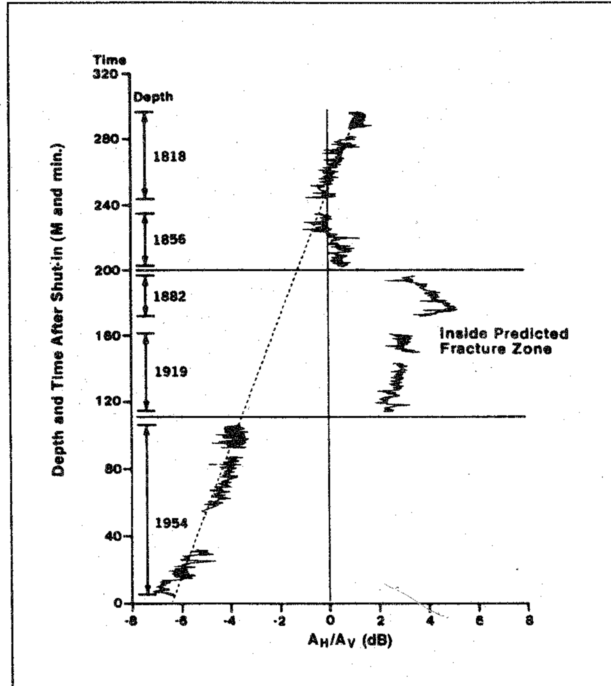

Fig. 2—The background motion A_H/A_V vs. time at the five depths at the SFE 1 in decibels relative to unity.

Data Acquisition. Microseismic logging requires a single downhole data-acquisition tool, a standard seven-conductor wireline and truck, standard data digitizing and recording equipment, and wellhead-pressure containment equipment if necessary. We record the complete (i.e., three-component) microseismic motion data along a traverse, which consists of a sequence of discrete depths in the well. We initially choose the traverse interval span from the fracture design and make adjustments from additional information, including formation and casing-bond factors. We record only when the well is quiescent and all surface activity is held in abeyance. We do not record during active pumping or stimulation. This is necessary to prevent noise contamination downhole. At each recording depth, the standard recording strategy is to lock the sonde, slack the wireline, record the data, take up the slack, unlock, and move to next depth recording.

The downhole monitoring tool consists of a three-component (i.e., three orthogonal geophone packages), vertical-seismic-profiling (VSP) -type motion-sensing sonde with a hole-lock mechanism and horizontal-azimuth-determination tool. In addition to the downhole tool, we place a geophone on the wellhead. This geophone, with the downhole geophones, aids in noise identification and removal. When pressured wells are logged (e.g., during postfracture shut-ins), a lubricator with grease injector also must be used.

Present data-acquisition technology is limited to a single, three-component tool on a standard seven-conductor wireline. Simultaneous, multiple-level, three-component data recording would be beneficial and would further enhance fracture diagnostics.

Examples

The results of a series of three field experiments follow: the Staged Field Experiments 1, 2, and 3 (SFE's 1, 2, and 3), sponsored by the Gas Research Inst. and performed in east Texas. These examples show the development of the height determination method. In addition to these operations, we have used both the height and azimuth methods successfully on wells in west Texas, New Mexico, Colorado, Wyoming, Michigan, Kansas, West Virginia, Louisiana, Alabama, and California.

SFE 1. In Dec. 1986, Teledyne Geotech participated in the SFE 1 in the Waskom field near Waskom in east Texas. The Travis Peak formation, a low-permeability, tight gas sandstone was targeted. Travis Peak contains intermittent zones of natural, vertical extension fractures. Many natural fractures are open and partly mineral-filled. The formation contains an extensive network of natural microfractures.[3]

We recorded data with the wellhead shut in during the first 4.5 hours after a minifracture of 127 m^3 of 30-lbm linear gel. We recorded data at 1954, 1919, 1882, 1856, and 1818 m, successively. **Fig. 1** indicates the amount of recording time at each depth.

Fig. 1 shows root-mean-square (RMS) time averages (10-second windows) of the amplitudes of the background motion as a function of time relative to shut-in. Well pressure was not recorded. The solid, straight-line segments in Fig. 1 indicate recording hiatuses.

The total-motion RMS time history is essentially a total recorded seismic-energy time history. In Fig. 1, the total-energy history seems to follow a smooth two-phase behavior: an initial steep decline followed by a much slower decline. The importance of this behavior lies in how it contrasts with the behavior of the individual component RMS. The horizontal and vertical component RMS's or energy levels (Fig. 1) do not follow the total-energy-history behavior. Note their relative shift in amplitudes at 1919 and 1882 m compared with the three other depths.

Note also in Fig. 1 that the data at the end of the recording session have flattened substantially. This indicates that they are approaching the ambient or stable level, which implies a useful recording window of approximately 3 to 4 hours.

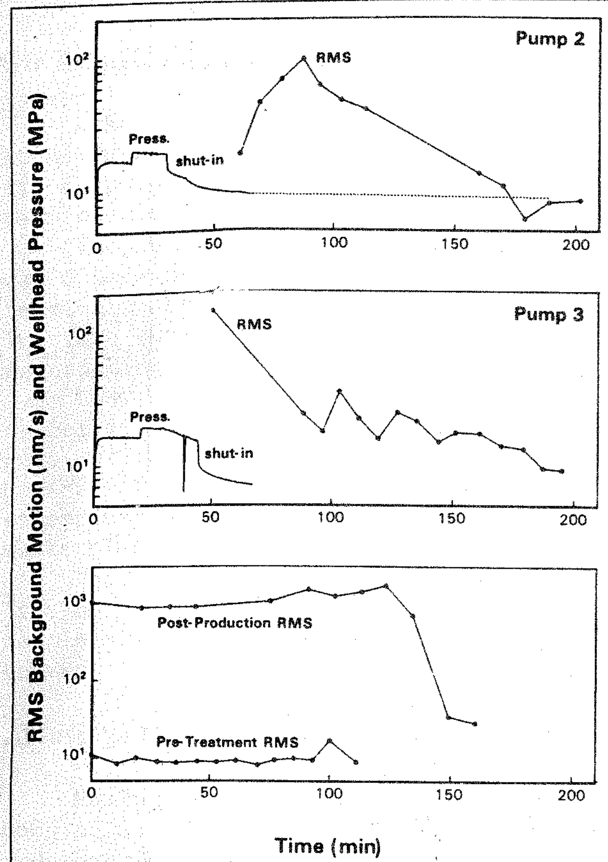

Fig. 3—Averaged RMS background motion amplitudes and wellhead pressure vs. time at SFE 2.

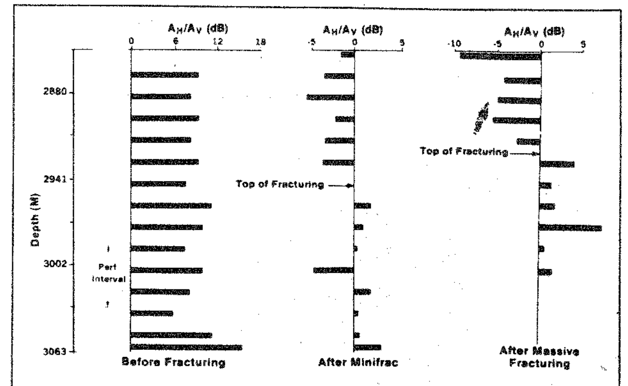

Fig. 4—Averaged A_H/A_V ratios as functions of recording depth at SFE 2.

To enhance the component anomalous behavior, we calculated background-motion A_H/A_V ratios directly. Because A_H/A_V is a ratio of simultaneous seismic components, it greatly reduces obfuscating elements in the data, including source time effects and poorly matched geophone components. **Fig. 2** shows the A_H/A_V vs. time and associated recording depths. As in Fig. 1, we calculated the data for Fig. 2 with 10-second RMS windows. The breaks in the data show the recording hiatuses. The dashed line in Fig. 2 is an "eyeball" fit to a continuous exponential trend between the first and last two recording depths. The A_H/A_V in Fig. 2 and subsequent figures are plotted in decibels [i.e., $10 \log_{10} (A_H/A_V)^2$].

Together, Figs. 1 and 2 show that the excursion or anomaly in the motion component behavior is an artifact of wave propagation through the local geology and not a vestige of changing seismic source characteristics. However, the implications of Figs. 1 and 2 require discussion. SFE 1 lacked a pretreatment, prefracture data baseline. As a result, the inversion of the A_H/A_V ratio cannot be linked unambiguously to the fracture treatment.

However, if we assume that the A_H/A_V inversion is caused by the treatment, as in subsequent wells, the anomaly bounds the vertical extent of the affected zone. The top occurred from 1856 to 1882 m and the bottom occurred from 1919 and 1954 m. An independent study of postfracture dimensions sited the top and bottom of the affected zone at about 1853 and 1939 m, respectively.[4]

SFE 2. SFE 2 began in mid-November 1987 at the Well SFE No. 2 in the North Appleby field near Nacogdoches, TX. Well SFE No. 2 is about 100-km south-southwest of Well SFE 1. As at SFE 1, the targeted formation was the Travis Peak but at a much greater depth (≈ 3000 m).

SFE 2 consisted of two minifractures and two massive fracture treatments. The first SFE 2 minifracture had three separate small-scale pumping episodes, with each followed by a wellhead shut-in. A few weeks after this minifracture, a second minifracture and two massive fracture treatments were performed.

We microseismically logged the treatment well at four different times: once before the first minifracture, twice during shut-ins of the first minifracture, and once after the massive treatments and some production. For these operations, we modified our recording strategy, greatly reducing the amount of time at each depth.

From the SFE 1 data, we learned that a few minutes of data per depth would be enough for accurate A_H/A_V determinations. Shortening recording time per depth allowed more recording depths, thereby increasing delineation of the A_H/A_V anomaly.

The well casing at SFE 2 was perforated from 2991 to 3032 m. We chose the recording interval to ensure that the fracture, which was predicted to extend from 2896 to 3082 m, would be enveloped. A stratigraphic section from neighboring wells projected a limestone layer beginning at 3082 m. This layer represented a barrier to downward fracture growth and was predicted to be the lowest point of the fracture. This prediction agrees with subsequent findings.

We recorded the pretreatment data in the liquid-filled, unpressurized well. Within minutes after completing this traverse, the first minifracture pumping stage (Stage 1) began. Immediately after Stage 1 (41 m^3 of 2% KCl water), a pressure leak developed in the wellhead and precluded logging. After the repairs, Stage 2 (72 m^3 of 2% KCl water) was pumped. After some delays and with the wellhead pressure shut in, we logged the well. The final pumping stage, Stage 3 (95 m^3 of 2% KCl water followed by 36 m^3 of brine-water flush), was performed, after which we again logged the well.

A few weeks after the first minifracture, a comparably sized second minifracture and two massive fracture treatments (approximately 100 000 m^3 of gel with sand) were performed. At the end of March 1988, we microseismically logged the well again. Between the massive treatments and relogging, the well had produced a small amount of gas and formation water.

Immediately before this final logging session, the well was backfilled with water. This required about 1000 vertical m of water, giving approximately 10 MPa of additional pressure to the affected zone. During logging, sand in the well bottom stopped the tool at 3013 m.

We processed the SFE 2 data with the same signal/background separation and analysis techniques as for the SFE 1 data. For easier interpretation and because of its consistent behavior, we present the results with a single, average RMS or A_H/A_V at each recording depth instead of the running windows of Figs. 1 and 2.

Fig. 3 shows the average background RMS time histories and the wellhead-pressure histories. The dashed line is a smooth data interpolation between measured values. As in Fig. 1, the data in Fig. 3 show combined temporal and spatial variations. For reference, the system noise level was about 3.0 nm/s.

Fig. 3 shows that the wellhead pressures after Stages 2 and 3 correlate only weakly with their corresponding microseismic RMS amplitude (energy) levels. Note the increase in RMS levels after Stage 2.

TABLE 1—RECORDING DEPTHS AND INITIATION TIMES AT SFE 3[5]

Depth (m)	Preperforation	Prefracture	Stage 1	Stage 2	Stage 3	Postmain Fracture	Perforations (m)
2652						24	
2667						23	
2682						22	
2697						20	
2713						1	
2720						21	
2728						2,19	
2736						3,18	
2743	24	6	6	6	6	4,17	
2751	23			19		5,16	
2758	22	7	7	7	7	15	
2766	21			18			
2774	20	5	5	5	5	6	
2781	19			17			
2789	18	8	8	8	8	14	
2795	17			16		13	
2804	16	4	4	4	4	7	
2818	15			20			2812
2819	14	10					2819
2822						8	
2825			9	9	9		
2827	13						2830
2835	12						
2842	11						2944
2850	10	11	10	10	10	12	
2858	9			15			
2865	8	3	3	3	3	9	
2873	7			21		11	
2880	6	12	22	11	11	10	
2888	5			14			
2896	4	2	2	2	2		
2903				22			
2911	3		12	12	12		
2918				13			
2923		1	1	1	1,13		
2926	2						
2929	1						
							Total Depth 2957 m

In general, we find poor correlation between the postpump RMS's and well-pressure histories, which is quite significant. The reasons for the lack of correlation are given below.

Fig. 4 shows average background motion A_H/A_V before the minifracture, after the minifracture, and after the massive fracturing. Each A_H/A_V in Fig. 4 was averaged from a set of A_H/A_V calculated with a 0.1-second window. The bar format in Fig. 4 simplified the presentation and interpretation.

Fig. 4 is significant. It compares the pre- and postfracture data sets and demonstrates a direct effect from the treatment. The pretreatment A_H/A_V show no characteristic anomaly, structure(s), variations, or inversions and show a consistent $A_H>A_V$ at all logged depths. In contrast, the post-treatment A_H/A_V show structure and a systematic variation with depth, similar to that implied at SFE 1. This anomaly is a direct artifact of the treatment.

Data logged at or above 2929 m indicate $A_V>A_H$ and, with minor exceptions, at and below 2944 m $A_H>A_V$. The inversion point in the post-treatment A_H/A_V profile is the boundary between the fractured and unfractured zones of the formation and gives the fracture height.

The post-massive-fracture data in Fig. 4 corroborate both existence and location of the anomaly in A_H/A_V. Fig. 4 shows the inversion in the A_H/A_V profile between 2914 and 2929 m. The data in Fig. 4 also indicate that the bottom of the fracture extended below the bottom of the well, as predicted.

SFE 3.[5] SFE 3 began in Dec. 1988 at Well SFE No. 3 in the Waskom field near Waskom, TX. The well is about 1.61 km from Well SFE 1. The target zone was the Taylor sandstone of the Cotton Valley formation, just below the Travis Peak formation. This experiment was to confirm the utility of the A_H/A_V anomaly and to compare the A_H/A_V results with more traditional borehole logs.

Before the perforation, cement-bond logging with roughly 14-MPa wellhead pressure indicated very good bonding between 2743 and 2926 m and slight degradation between 2679 and 2743 m. A second bond log with the well unpressurized indicated considerable bond degradation over the entire interval. The bottom of the well was at 2957 m.

We microseismically logged Well SFE No. 3 six times. The first was a preperforation traverse consisting of 24 monitoring depths from 2743 to 2929 m (**Table 1**) with the well shut in and pressurized at about 14-MPa wellhead pressure. The well casing then was perforated from 2812 to 2819 m and from 2830 to 2844 m.

We then recorded a preminifracture, postperforation microseismic log at 11 depths (2743 to 2923 m, Table 1). Before logging, the formation was taking fluid. The well was pressurized immediately before logging and held at a constant wellhead pressure (≈ 7 MPa) during logging to improve the casing/formation coupling. Holding this perforated well at constant pressure (i.e., pumping fluid into the well) resulted in borehole fluid movement, which affected the sonde and created very noisy data.

The following morning, a three-phase minifracture was performed. After each phase, the well was shut in and microseismically logged. During the pumping of each phase, the sonde was locked at the bottom of the well to avoid obstructing the treatment fluid flow.

Fig. 5 shows the bottomhole pressure (BHP) measured throughout the treatment. Stage 1 of the treatment consisted of approximately 72 m^3 of 40-lbm linear gel. At pumping completion, we logged a 12-depth Stage 1 traverse (Table 1). Stage 2 pumping (143 m^3 of 40-lbm linear gel) began after logging (Fig. 5). Immediately after this pump, we logged a 22-depth Stage 2 traverse (Table 1).

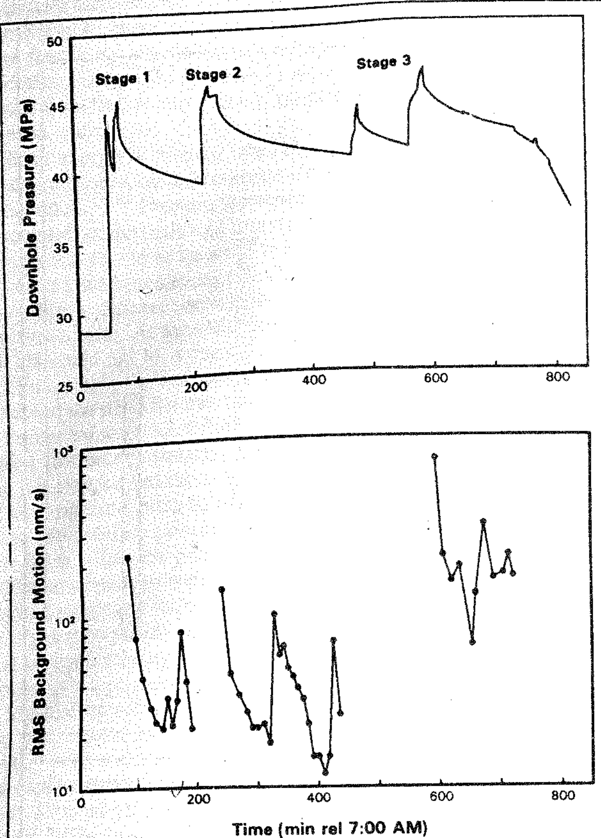

Fig. 5—BHP and averaged RMS background motion amplitudes vs. time at SFE 3. Min rel = minutes relative.

A pump-truck breakdown at the beginning of the Stage 3 pumping caused a 1-hour delay (Fig. 5). At completion, Stage 3 consisted of 72 m^3 of crosslink gel followed by 48 m^3 of 2% KCl water. At pumping completion, we logged a 12-depth Stage 3 microseismic traverse (Table 1).

The bottom panel in Fig. 5 shows the average total background motion RMS as a function of time during the minifracture shut-ins. Neighboring time points do not represent neighboring depth points (Table 1). However, Fig. 5 does show a weak correlation between downhole pressure and motion energy levels. Both show a long-term decline. But, in the short term, the RMS behavior indicates that pressure is not the only factor affecting the recorded seismic energy level.

In mid-March 1989, Well SFE No. 3 had a massive hydraulic fracture treatment. This included about 207 m^3 of KCl water; 525 m^3 of 50-lbm crosslink gel; 1177 m^3 of 40-lbm gel, of which 938 m^3 was crosslinked; 5715 kg of 100-mesh sand; and about 5×10^5 kg of 20/40-mesh Ottawa sand.

Between March and late July, the well was backflowed, produced, and shut in for pressure-buildup tests. In late July 1989, we logged the final, 20-depth "postmain" microseismic traverse (Table 1). Immediately before this survey, the well was partially backfilled with about 2000 (vertical) m of water. Halfway through the survey, the well again was backfilled with water during recording hiatuses. In retrospect, this backfilling may have been an error in judgment. The fluid motion from the backfilling generated a high noise level. However, backfilling was required for well maintenance.

Fig. 6 shows average total background RMS amplitudes before the main fracturing as a function of recording depth. We do not present the postmain data because of the backfilling-noise contamination.

Fig. 6 shows smooth variations in the pretreatment data and sporadic, nonsystematic variations in post-treatment data. This behavior corresponds to the excessive noise encountered. Besides 60-Hz electrical noise, we think the noise resulted from fluid invading the annulus between the casing and the formation. The near uniformity in the pretreatment RMS's and the inconsistencies in the traditional logs, described below, corroborate this hypothesis.

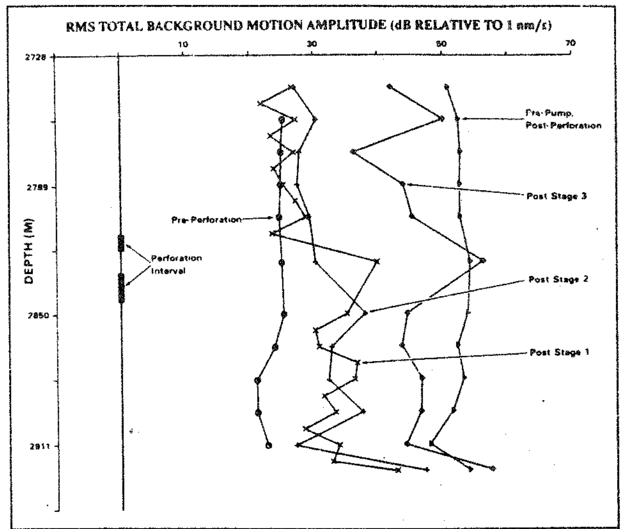

Fig. 6—Total background motion RMS's vs. depth at SFE 3.

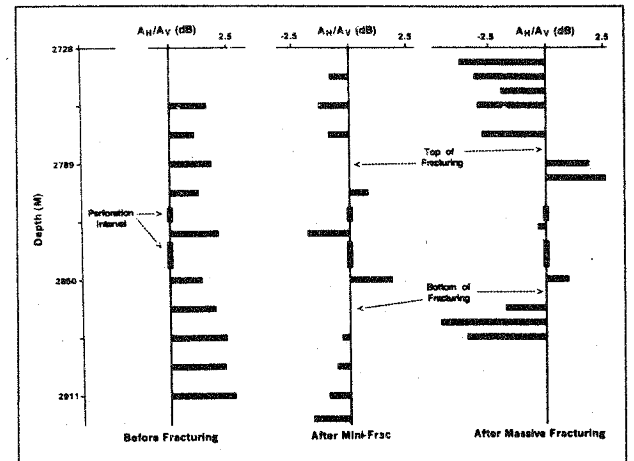

Fig. 7—Averaged RMS A_H/A_V ratios vs. depth at SFE 3.

Although the data had extensive noise contamination, because of the robustness of the A_H/A_V method, the anomaly survived noise-removal processing. **Fig. 7** shows representative pretreatment, cominifracture, and postmassive-fracture results of the A_H/A_V analyses on the SFE 3 data. In the figure, the pretreatment result was from preperforation pressurized data and the cominifracture was from Stage 3 shut-in data.

In general, the results in Fig. 7 corroborate the results from the previous experiments. The pretreatment A_H/A_V do not show the inversion anomaly. Both post-treatment data sets show the anomaly or, equivalently, the vertical signature of the fracture.

Fig. 7 results agree quite well with openhole stress testing performed before casing.* This testing determined a minimum stress vs. depth profile for the well. This profile showed a substantially lower-stress region surrounding what became the perforation depths. Going downhole, the top of the lower-stress zone, defined by a relative decrease of 5.9 MPa, occurred at 2795 m. The bottom of the zone, defined by a relative stress increase of 10.0 MPa, occurred at 2878 m. A second stress increase, defined by an additional 7.6 MPa, occurred at 2886 m. In this lower-stress region, a small sub-

*Personal communication with E. Hunt, ResTech, Houston (1989).

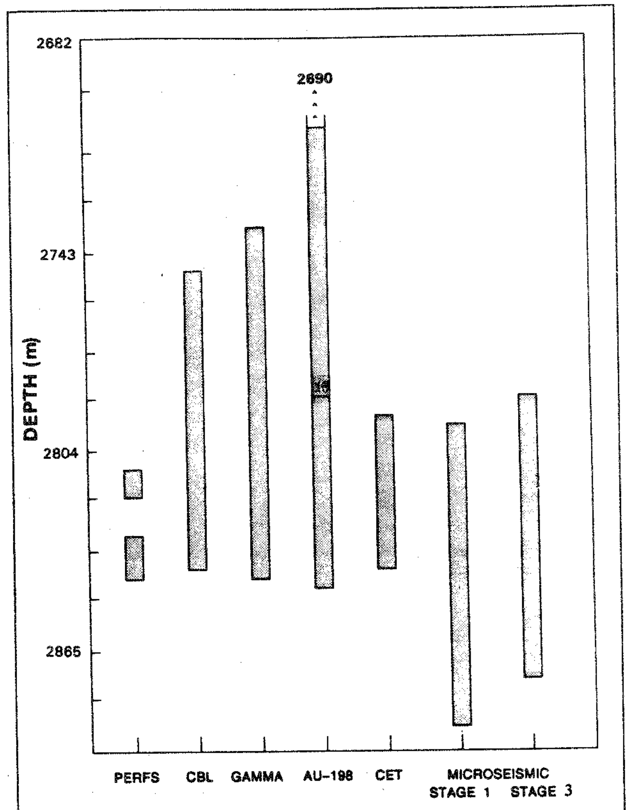

Fig. 8A—Traditional and microseismic logging results at SFE 3, postminifracture. ⋮ = data continues upward to the indicated depth.

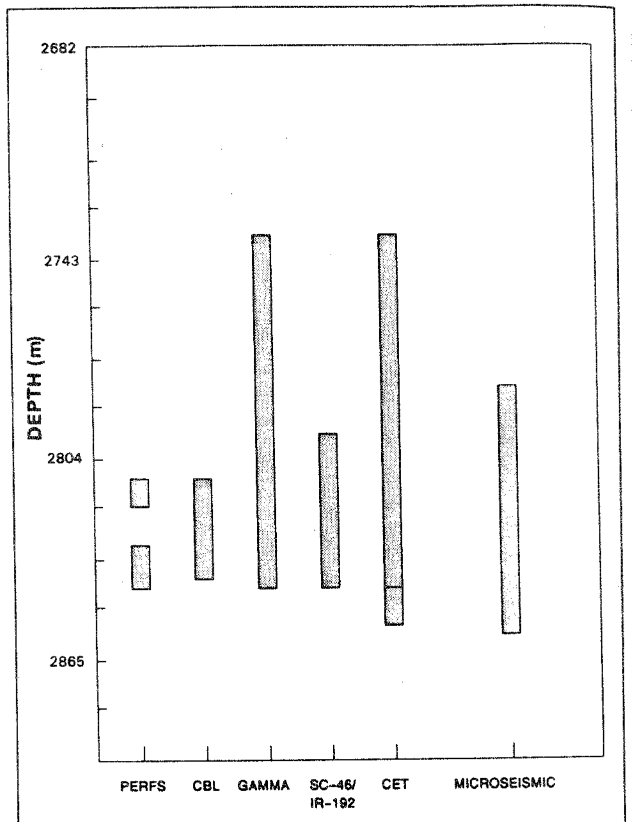

Fig. 8B—Traditional and microseismic logging results at SFE 3, postmain fracture.

zone between 2847 and 2861 m showed a step increase of about 8.0 MPa. The smaller postmassive-treatment height is probably the result of sand proppant reducing the reach of the treatment fluid and amplifying the effect of the intermediate stress step.

Besides demonstrating the A_H/A_V anomaly, SFE 3 was particularly important because of a suite of traditional logs done pre- and postminifracture, postmassive-fracture treatment, and postproduction. The postminifracture logs were done within 1 or 2 days of the first minifracture. As in the microseismic survey, the postmassive-fracture logs were recorded during 2 days in late July after the mid-March treatment.

Figs. 8 gives interpretations of fracture-induced (height) anomalies from the well logs. Fig. 8A shows the postminifracture data. Fig. 8B shows the postmain-fracture data. The logs included cement bond, natural gamma ray, gold-198 (AU-198) -tracer scan, cement evaluation tool (CET), and scandium-46 (SC-46)/iridium-192 (IR-192) -tracer scan logs. Fig. 8 shows that these logs generally interpret the bottom of the fracture near the bottom of the perforations. This is about 3 m above the top of the intermediate-stress barrier, at 2847 m. The cement bond, gamma ray, and gold-tracer logs give the (fracture) top well above the highest-stress barriers. These particular anomalies are thought to result from fluid invasion and microfracturing in the casing-formation annulus. In general, Fig. 8 shows that these conventional logging methods are inconsistent and seem unsuitable for height determination.

Theory and Simulations

Conceptual Model. Traditionally, hydraulic fracture modeling begins with a high-pressure fluid injected into a stressed, homogeneous, impermeable medium. The result is Mode 1 or planar fracturing with two slender, symmetric wings growing from the wellbore and opening against the least principal stress. At typical treatment depths (i.e., >1000 m), this modeling necessarily predicts a vertical or near-vertical fracture plane.

In actuality, formations are porous; treatment fluids are forced (euphemistically called "leakoff") into the pores. In saturated formations, the treatment fluid acts as a piston, displacing the in-situ fluids and elevating their pressures. In this picture, the fracture is now in a narrow leakoff zone (i.e., the treatment-fluid-invasion zone). Because of in-situ stresses, leakoff or invaded zones are stress-aligned, tabular ellipsoids. Field studies suggest that leakoff zones are 0.1 m or less wide.* Because leakoff zones are narrow, the pressure in the zone drops off only slightly from the pressure in the fracture. Because the fracture fluid is overpressured (i.e., greater than the least principal in-situ stress), the leakoff zone is at pressures great enough to dilate formation pores and, arguably, cause secondary fracturing.

However, a fracture-with-leakoff-dilatation model also is incomplete and insufficient for this work. This model does not explain many characteristics of the microseismicity,[6-11] including the lateral extent of the source cloud and its activation history. Microseismicity is induced after pumping, a few hours into the shut-ins,[12] and after backfilling previously fractured wells.

Mahrer and Mauk[12] used displacement and pressurization of the formation fluid in place by the leakoff fluid to explain some of the microseismic characteristics. They surrounded the fracture and leakoff zone with a much wider (i.e., up to tens of meters) seismic low-velocity zone. This zone is defined as the region containing the pressurized formation fluids.[13] In this region, the seismic velocity reduction is the result of pore dilatancy from the pressurized fluid—a well-established mechanism of reducing seismic velocities.[14-17] The Mahrer and Mauk model showed that this low-velocity zone acted as a seismic wave-guide, confining and substantially altering the waveforms recorded in the treated well.

The conceptual model proposed here is an expansion of the Mahrer and Mauk model. The original model is extended to explain more of the microseismicity characteristics. This new model postulates three seismic source types active after wellbore pressure changes (e.g., pumping): shear-strain energy release remote to the new fracturing, elastic-strain recovery or rebound, and thermal microfracturing. The presence or absence of any of these sources results from factors only partially understood and seems to be unique to each setting.

Shear energy is released when fluid pressure across a plane exceeds the Mohr-Coulomb criterion and when the locked in-situ shear is liberated.[18,19] Pressure movement in the new fracturing and the associated transmission of pressure into the formation from this movement seem to be the mode to induce seismicity. We have found in remote well monitorings that this source mechanism seems to cause large, discrete events at the edges or just outside the primary fractured zone. At the well separations of these studies, smaller events could not be recognized above ambient noise.

The second proposed source mechanism is strain recovery or rebound of the strain the treatment put in the rock. Rock matrix strain is recovered when local fluid pressure becomes less than the confining (formation) stresses. This should begin after active pumping has stopped and fluids diffuse (i.e., close fractures). Because of local pressure gradients in the fracture, this mechanism can continue after surface pressures indicate that the downhole pressure has fallen below the presumed closure pressures.

If strain recovery were the only post-treatment source mechanism, background motion RMS's would follow the inverse root time/pressure-decline history of shut-ins.[20] As discussed, the seismic energy level may follow a different behavior. The third postulated source type, thermal microfracturing, may cause this behavior.

Thermal microfracturing is caused by the combination of heating and expanding fracture fluid and cooling and contracting rock,[21] with the added factor of the high-pressure fluid invading and expanding newly microfractured surfaces. In a gel fracture treatment, thermal gel expansion is estimated at between 2 vol% and 4 vol%.* The tensile stress created by thermal contraction of a typical reservoir rock is estimated at about 0.15 MPa/°C.** Nucleation and growth of thermally induced microfractures have been demonstrated theoretically[22] and experimentally at laboratory scale.[23]

Together, these mechanisms would be expected to form a cloud of source events. These sources will be distributed in space, time, and size or individual energy release. The cloud is pervasive to the fracturing. We expect the cumulative population distribution or the b-value distribution[24] to be inversely proportional to size, as are earthquake aftershocks.

Aftershocks follow a b-value or Gutenberg and Richter-type relationship[25]: $\log N=a-bM$, where N=the cumulative number of events of size M or smaller and a and b=empirically derived constants. Scholz[25] showed that this relation holds for microfracturing in laboratory rock samples and gave b values between 0.1 and 2.6. For reference, b typically is about 1.0 for earthquake aftershocks.

Because we are limited to use of a single sonde in the treated well, we cannot find events and unambiguously determine their source sizes (i.e., close small events can look like large, distant events). As a result, we cannot calculate a b value for the recorded microseismicity and can only make reasonable hypotheses.

With these sources, we hypothesize an in-situ picture of an extended fractured volume containing multiple fractures in the extended, pressure-driven dilatancy envelope. Although we cannot demonstrate this with my data, we think that multiple fracturing instead of planar fracturing should occur for at least four reasons. First, as discussed later, field data substantiate use of multiple fracturing instead of planar fracturing. Second, fluid pressure lateral to the principal fracture growth is still overpressured and great enough to fracture the rock. Third, thermal microfracturing is unavoidable and will introduce residual fracturing.[22] And fourth, geologic formations are heterogeneous, which means pervasive weaknesses, fractures, faults, joints, bedding planes, etc., occur at a range of scales.

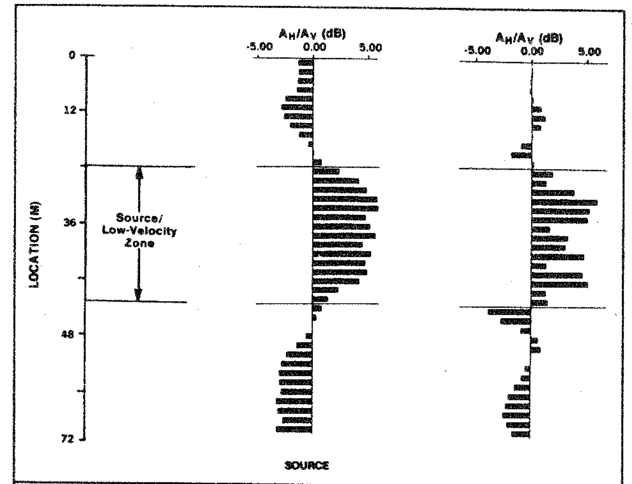

Fig. 9—Synthetic A_H/A_V ratios vs. location.

Fracturing a heterogeneous material unavoidably produces fractures that are not necessarily in the large-scale, intermediate/greatest principal-stress plane and are not necessarily planar. This includes, for example, *en echelon* fracture growth along intersecting planes of new and pre-existing surfaces.[25] In addition, heterogeneous fracture growth is unstable and easily bifurcates.[22,26-29] Some studies view naturally occurring hydraulic fractures as a fractal network.[30]

The concept of a multiple-fractured, hydraulically communicating region has been corroborated by field studies. Multiple, vertical fractures extending from the wellbore were found in Well SFE No. 2 overcores recovered after a small (<10 vertical m of water) stress test before casing the well.[31] A stress-aligned, multiple-fractured zone has been reported in a mineback experiment after a hydraulic fracture.[32]

Seismic studies have found elongated, stress-aligned microseismic (hypocentral) clouds during cotreatment seismic monitorings from neighboring observation wells at Los Alamos' Hot Dry Rock experiments in New Mexico[6,8-10,33] and at fracture treatments in Alabama.* Fehler *et al.*[8] and Fehler[34] fit the New Mexico hypocenters to a series of intersecting planes that individually were not parallel to the principal direction of the overall hypocentral cloud. They concluded that these planes represented the joint structure of the fractured granite. These findings concur with post-treatment VSP and cross-hole seismic surveys done in England,[35] which also found an overlay between a low-velocity anomaly and the microseismic cloud.

These arguments culminate in a phenomenological picture of a hydraulic fracture zone that, after pressurization, is a dynamic, nonequilibrium, nonisothermal, seismically active, low-velocity zone. The zone includes an interlocking network of pressurized surfaces (new and old) and pores. The network is in hydraulic communication with the wellbore through the perforations. In general, the zone is stress-aligned and to first order is probably a narrow, blunted shape, possibly an ellipsoid, teardrop[36] or something slightly more exotic, governed by in-situ stress variations.[37]

The zone width may be very small compared with the length and height (>0.01%) if the multiple fracturing and dilatancy are strongly contained by low-permeability, high formation stresses and low treatment pressure.[4] In this setting, the fracturing will be most nearly single-planar. Similarly, the width may be large (5% or more) if the formation is weak,[26] highly permeable, or fragmented or if treatment pressure is high.

This picture of hydraulic fracture and the studies cited also indicate that the seismicity used for the A_H/A_V calculations are not just those events near the casing. First, the microseismicity pervades the fracture. Second, the frequencies of the background motion data are from 50 to approximately 300 Hz, and the seismic velocities are a few thousand meters per second. Attenuation should allow a minimum of three wavelengths of propagation before the small-

*Personal communication with M. Struhbar, Mobil Oil Co. (1986).

*Personal communication with B. Robinson, S.A. Holditch & Assocs. Inc. (1988).
**Personal communication with K. Heffer, BP (1989).

*Unpublished study, Teledyne Geotech (1987).

event energy is absorbed and masked by the noise. Because velocity is the product of wavelength times frequency, seismicity with wavelengths of 10 m is used. This argues that formation penetration of the A_H/A_V method can be about 30 m or more from the wellbore.

A_H/A_V Computer Simulations. To test this model for an A_H/A_V anomaly, we ran a series of computer models. The modeling method was a finite-difference code[12] that uses a second-order discretization of the 2D, elastic motion equations.[38] We tailored the code specifically to synthesize seismic background motion. This included an optional low-velocity zone embedded in the unaffected formation and a microseismic source cloud. The model does not include tube waves.

We ran many computer simulations and settings. **Fig. 9** shows synthetic A_H/A_V ratios vs. local wellbore site from two representation simulations: a microseismic source cloud in an unaffected formation and a microseismic source cloud in a low-velocity zone embedded in an unaffected formation. For direct comparison, we used the same source configuration for both examples.

For Fig. 9, we used P- and S-wave velocities in the rectangular low-velocity zone at 53% and 46%, respectively, of the P and S velocities of the unaffected formation rock. These values represent the reasonable extremes for velocity reduction. We used other velocity structures and found analogous results. The computer runs were not designed specifically to simulate the SFE settings but instead to investigate the A_H/A_V anomaly.

We calculated the A_H/A_V ratios in Fig. 9 in the same manner as the field data, except that the synthetic horizontal data had only one component because the code was 2D. Fig. 9 brings out three significant points. First, the same A_H/A_V inversion anomaly found in the field data is found in the synthetics. Second, the inversion is most directly the result of the cumulative effect of a source cloud. This explains why the anomaly is in the pervasive background motion but eludes the discrete event analysis. For example, in computer runs with a low-velocity zone and a single source or a single source without a low-velocity zone, we found no discontinuous A_H/A_V inversion. Third, the top and bottom of the $A_H > A_V$ region represent the limits of the treatment-altered region or, equivalently, the height of the affected zone.

Because of the utility of the A_H/A_V anomaly as a diagnostic tool, further clarification regarding the importance of the low-velocity zone is necessary. The "source only" model in Fig. 9 seems to show that the A_H/A_V inversion sites give the height of the source cloud, obviating the presence or need of a low-velocity zone. This is somewhat misleading. For the result shown, the source cloud borders the simulated sonde recording traverse. For simulations in which the recording traverse was more distant from the source region, the A_H/A_V inversion points became more separated, diverging from the actual source cloud height. This spreading is an artifact of the geometric spreading of the source energy. However, for simulations that included the low-velocity zone, the geometric spreading was not a factor. The low-velocity zone acted as a wave-guide containing enough energy to maintain A_H dominance over A_V in its boundaries. In this regard, Fig. 9 offers a strong theoretical argument for the interpretation that the A_H/A_V anomaly delineates the zone altered by a hydraulic fracture treatment.

Conclusions

1. A new method that determines the azimuth and height of the fractured zone produced by a hydraulic fracture treatment was developed. The method uses the microseismic motion data generated in the affected zone and recorded in the cased treatment well. The method is particularly appealing for a number of reasons. First, no other reliable methods, including traditional logs, work in cased wells. Second, the method is based on a robust, broadband anomaly in the data. Third, because the microseismic sources are spatially pervasive over the fracture, the method looks much deeper into the formation than traditional logging methods. Fourth, the data-acquisition phase of the method is performed with existing technology, with a minimum of obstructions to normal well operations, and without damaging the well.

2. The method used to determine the fracture azimuth is based on identifying the direction of particle motion polarization of the initial phase of the larger, discrete seismic events. The vector of polarization aligns with the fracture azimuth. This is a method established from earthquake studies.

3. The method used to determine the fracture height is new. It relies on identifying a change in the dominant direction of motion in the background data. The delineation of this anomaly maps the vertical extent or fracture height.

4. To date, these methods have been used on more than 24 operations at different depths and in different formations. In some cases, we recorded immediately after a treatment, during shut-in; in other cases, we recorded several months after completion, including a series of treatments, and some well production. In all cases, before data recording, fluid (i.e., treatment fluid or water) was added or withdrawn (not discussed) to the treatment-affected region to induce microseismicity.

Nomenclature

a = empirical constant in Gutenberg and Richter relationship[25]
A_H = horizontal average vector component amplitude
A_V = vertical average vector component amplitude
b = empirical constant in Gutenberg and Richter relationship, typically about unity for earthquakes recorded at the surface of the Earth
M = magnitude (size) of individual sources in a source cloud
N = cumulative number of seismic events within a source cloud

Acknowledgments

We performed this work while employed at Teledyne Geotech and acknowledge J. Fix (Teledyne Geotech) for his interpretations of the well logs at the SFE 3 experiment and A. Kalik (Teledyne Geotech) for proofreading this manuscript. Funding for this research was provided by the Gas Research Inst. under Contract 5087-211-1624. As of April 1991, the A_H/A_V method has been patented in the U.S.

References

1. Aronstam, P.S. and Yasuda, A.K.: "A New Generation of Borehole Receivers," Expanded Abstracts of the Technical Program, *Proc.*, Soc. Exploration Geophysicists, 57th Annual Intl. Meeting and Exposition, New Orleans (1987) 782–85.
2. Gal'perin, E.I.: *The Polarization Method of Seismic Exploration*, Reidel Publishing Co., Boston (1977).
3. Laubach, S.E., Baumgardner, R.W. Jr., and Meador, K.J.: "Analysis of Natural Fractures and Borehole Ellipticity, Travis Peak Formation," Topical Report (July 1986–May 1987) GRI-87/0211, Bureau of Economic Geology, U. of Texas, Austin (1987).
4. Cleary, M.P.: "The Engineering of Hydraulic Fractures—State of the Art and Technology of the Future," *JPT* (Jan. 1988) 13–21.
5. Robinson, B.M. *et al.*: "Hydraulic Fracturing Research in East Texas: Third GRwe Staged Field Experiment," *JPT* (Jan. 1992) 78–87.
6. Batchelor, A.S., Baria, R., and Hearn, K.: "Monitoring Effects of Hydraulic Stimulation by Microseismic Event Location: A Case Study," paper SPE 12109 presented at the 1983 SPE Annual Technical Conference and Exhibition, San Francisco, Oct. 5–8.
7. Pine, R.J. and Batchelor, A.S.: "Downward Migration of Shear in Jointed Rock During Hydraulic Injections," *Intl. J. Rock. Mech. Min. Sci., Geomech. Abst.* (1984) **21**, 249–63.
8. Fehler, M., House, L., and Kaieda, H.: "Determining Planes Along Which Earthquakes Occur, Method and Application to Earthquakes Accompanying Hydraulic Fracturing," *J. Geophys. Res.* (1987) **92**, 9407–14.
9. Green, A.S.P. and Baria, R.: "Active Seismic To Determine Reservoir Characteristics of a Hot Dry Rock Geothermal System," paper presented at the 1987 Workshop of Geothermal Reservoir Engineering, Stanford U., Stanford, CA.
10. House, L.: "Locating Microearthquakes Induced by Hydraulic Fracturing in Crystalline Rock," *Geophys. Res. Let.* (1987) **14**, 919–21.
11. Parker, R.: "The Camborne School of Mines Hot Dry Geothermal Energy Project," *Scientific Drilling* (1989) **1**, 34–41.

12. Mahrer, K.D. and Mauk, F.J.: "Seismic Wave Motion for a New Model of Hydraulic Fracture With an Induced Low-Velocity Zone," *J. Geophys. Res.* (1987) **92**, 9293–9309.
13. Biot, M.A., Massé, L., and Medlin, W.L.: "A Two-Dimensional Theory of Fracture Propagation," *SPEPE* (Jan. 1986) 17–30.
14. Banthia, B.S., King, M.S., and Fatt, I.: "Ultrasonic Shear-Wave Velocities in Rock Subjected to Simulated Overburden Pressure and Internal Pore Pressure," *Geophysics* (1965) **XXX**, 117–21.
15. Todd, T. and Simmons, G.: "Effect of Pore Pressure on the Velocity of Compressional Waves in Low-Porosity Rock," *J. Geophys. Res.* (1972) **77**, 3731–43.
16. Christensen, N.I. and Wang, H.F.: "The Influence of Pore Pressure and Confining Pressure on Dynamic Elastic Properties of Berea Sandstone," *Geophysics* (1985) **50**, 207–13.
17. Nur, A.M. and Wang, Z.: *Seismic and Acoustic Velocities in Reservoir Rocks, Vol. 1, Experimental Studies*, Geophysics Reprint Series, Soc. of Exploration Geophysicists, Tulsa (1989) **10**.
18. Hubbert, M.K. and Rubey, W.W.: "Role of Fluid Pressure in Mechanics of Overthrust Faulting," *Geol. Soc. Amer. Bull.* (1959) **70**, 115–66.
19. Jaeger, J.C. and Cook, N.G.W.: *Fundamentals of Rock Mechanics*, Chapman & Hall Publishers, London (1989).
20. Howard, G.C. and Fast, C.R.: *Hydraulic Fracturing*, Monograph Series, SPE, Richardson, TX (1970) **2**.
21. McTigue, D.F.: "Thermoelastic Response of Fluid-Saturated Porous Rock," *J. Geophys. Res.* (1986) **91**, 9533–42.
22. Nemat-Nasser, S. and Keer, L.M.: "Thermally and Hydraulically Induced Tension Cracks," final report, Hot Dry Rock Reservoir Characterization and Modeling (Oct. 1, 1978–Sept. 30, 1979), LA-8343-MS, Los Alamos Scientific Laboratory, Los Alamos, NM (1980).
23. Dundurs, J.: "Laboratory Studies of Hydraulic and Thermal Fracturing," final report, Hot Dry Rock Reservoir Characterization and Modeling (Oct. 1, 1978–Sept. 30, 1979), LA-8343-MS, Los Alamos Scientific Laboratory, Los Alamos, NM (1980).
24. Bullen, K.E. and Bolt, B.A.: *An Introduction to the Theory of Seismology*, fourth edition, Cambridge U. Press, New York City (1985) 498.
25. Scholz, C.H.: "The Frequency-Magnitude Relation of Micro Earthquakes in Rock and Its Relation to Earthquakes," *Bull. Seismic Soc. Amer.* (1968) **58**, 399–415.
26. Keer, L.M., Nemat-Nasser, S., and Oranratnachai, A.: "Unstable Growth of Thermally Induced Interacting Cracks in Brittle Solids, Further Results," *Intl. J. Solids and Structures* (1978) **15**, 111–26.
27. Keer, L.M. and Chen, S.H.: "The Intersection of a Pressurized Crack With a Joint," *J. Geophys. Res.* (1981) **86**, 1032–38.
28. Nemat-Nasser, S., Keer, L.M., and Parihar, K.S.: "Unstable Growth of Thermally Induced Interacting Cracks in Brittle Solids," *Intl. J. Solids and Structures* (1978) **14**, 409–30.
29. Nemat-Nasser, S., Sukmi, Y., and Keer, L.M.: "Unstable Growth of Tension Cracks in Brittle Solids, Stable and Unstable Bifurcations, Snap-Through and Imperfection Sensitivity," *Intl. J. Solids and Structures* (1980) **16**, 1017–35.
30. Chiles, J.P.: "Fractal and Geostatistical Methods for Modeling of a Fracture Network," *Math. Geol.* (1988) **20**, 631–54.
31. Whitehead, W.S.: "In-Situ Stress Profile," presented at the 1989 Gas Technology Symposium, Dallas, June 7–9.

Author

Kenneth D. Mahrer has been principal scientist at the Southwest Research Inst. in San Antonio, TX, since 1991. Previously, he worked as a senior research geophysicist at Teledyne Geotech. Mahrer began his career at Stanford U., where he earned a PhD degree in geophysics. After graduation, he was awarded North Atlantic Treaty Organization and Natl. Science Foundation postdoctoral fellowships to the U. of Sheffield, England, and Northwestern U., respectively. These were followed by an assistant professorship at the U. of New Mexico. Mahrer is serving his second term as associate editor of *Geophysics*, the journal of the Society of Exploration Geophysicists.

32. Warpinski, N.R. and Teufel, L.W.: "Influence of Geologic Discontinuities on Hydraulic Fracture Propagation," *JPT* (Feb. 1987) 209–20.
33. Bame, D.A. and Fehler, M.C.: "Observations of Long-Period Earthquakes Accompanying Hydraulic Fracturing," *Geophys. Res. Let.* (1986) **13**, 144–52.
34. Fehler, M.: "Stress Control of Seismicity Patterns Observed During Hydraulic Fracturing Experiments at the Fenton Hill Hot Dry Rock Geothermal Energy Site, New Mexico," *Intl. J. Rock. Mech. Min. Sci., Geomech. Abst.* (1989) **26**, 211–19.
35. Green, A.S.P., Baria, R., and Jones, R.: "VSP and Cross-Hole Seismic Surveys Used To Determine Reservoir Characteristics of a Hot Dry Rock Geothermal System," paper presented at the 1987 Workshop on Forced Fluid Flow Through "Strong" Fractured Rock Masses, Garchy, France.
36. Weertman, J.: "Theory of Water-Filled Crevasses in Glaciers Applied to Vertical Magma Transport Beneath Oceanic Ridges," *J. Geophys. Res.* (1971) **76**, 1171–83.
37. Pollard, D.D.: "On the Form and Stability of Open Hydraulic Fractures in the Earth's Crust," *Geophys. Res. Let.* (1976) **3**, 513–16.
38. Kelly, K.R. *et al.* "Synthetic Seismograms: A Finite Difference Approach," *Geophysics* (1976) **41**, 2–27.

SI Metric Conversion Factors

Å	× 1.0*	E−01	=	nm
ft	× 3.048*	E−01	=	m
ft^3	× 2.831 685	E−02	=	m^3
lbm	× 4.535 924	E−01	=	kg
psi	× 6.894 757	E+00	=	kPa

*Conversion factor is exact.

SPEFE

Original SPE manuscript received for review April 15, 1991. Revised manuscript received March 30, 1992. Paper accepted for publication April 7, 1992. Paper (SPE 21834) first presented at the 1991 SPE Rocky Mountain Regional/Low Permeability Reservoirs Symposium held in Denver, April 15–17.